Published in final edited form as:
Psychiatry Res. 2011 December 30; 194(3): 354–362. doi:10.1016/j.pscychresns.2011.05.004.

Default Mode Network Dysfunction in Adults with Prenatal Alcohol Exposure

Priya Santhanam[1,*], **Claire D. Coles**[2], **Zhihao Li**[1], **Longchuan Li**[1], **Mary Ellen Lynch**[2], and **Xiaoping Hu**[1]

[1]Department of Biomedical Engineering, Georgia Institute of Technology/Emory University, Atlanta, GA 30322, United States.

[2]Department of Psychiatry and Behavioral Sciences, Emory University School of Medicine, Atlanta, GA 30322, United States.

1. INTRODUCTION

Neurocognitive deficit and social and adaptive dysfunction have been observed in individuals with prenatal alcohol exposure (PAE) (Guerri, et al. 2009; Mattson and Riley 1998). Adolescents with PAE generally have lower IQ, often accompanied by impaired visuo-spatial, attentional, verbal learning, and memory abilities (Coles, et al. 1997; Conry 1990; Mattson, et al. 1998; Olson, et al. 1998). While behavioral studies have extensively documented deficiencies in individuals with PAE, the underlying neuronal causes of the outcomes are still not well understood. There are only a few functional neuroimaging studies of the PAE population, and these mainly focus on the task-positive activation patterns created by the blood-oxygen level dependent (BOLD) response in functional MRI (fMRI). Two studies of spatial working memory have revealed functional differences in several task-associated brain regions in children and adults with fetal alcohol effects (Malisza, et al. 2005; Spadoni, et al. 2009). Additionally, a study of verbal learning in children with heavy PAE found exposed children had altered patterns of activation during a paired association task (Sowell, et al. 2007), while a separate study of response inhibition found BOLD differences in children and adolescents with heavy PAE (Fryer, et al. 2007). Two recent studies investigated arithmetic-related processing in prenatally exposed populations. Santhanam, et al. (2009) found less activation in calculation-associated regions in adults with dysmorphic PAE, while Meintjes, et al. (2010) reported additional activation in exposed children (as compared to control children) during a proximity judgement task and more dispersed activation during an exact addition task. Though these studies do report specific task-related changes in BOLD response in the PAE population, they do not examine the possibility of altered underlying global attentional modulation.

Recent discovery of consistent regions that are more active during resting periods than during cognitive demand has led to the characterization of a so-called “default mode network” (DMN) in the brain (Greicius, et al. 2003). Comprised primarily of the medial prefrontal cortex (MPFC), posterior cingulate cortex (PCC), precuneus, inferior parietal lobules (IPL), and medial temporal regions, the network has been shown to exhibit reduced activation in the presence of high cognitive demand (Golland, et al. 2008; Greicius, et al. 2003; Margulies, et al. 2007). Several studies have shown that DMN deactivation increases

Corresponding author: Xiaoping Hu, PhD Hospital Education Annex Biomedical Imaging Technology Center 531 Asbury Circle, Suite 305 Atlanta, GA 30322 Phone: (404) 712-2615 Fax: (404) 712-2707 xhu@bme.gatech.edu.
*present affiliation: Department of Neurology, The University of Chicago, Chicago, IL 60615, United States.

There are no conflicts of interest, including specific financial interests and relationships and affiliations relevant to this manuscript.

with increased task difficulty (McKiernan, et al. 2006; Singh and Fawcett 2008), and that activity persists during simple sensory tasks, in which good task performance is achievable with little attentional resources (Greicius, et al. 2003; Wilson, et al. 2008). Attention lapse, marked by longer reaction time and lower accuracy on an attentional control task, has been associated with less task-induced deactivation of the DMN (Weissman, et al. 2006). Thus patterns of task-related DMN activity are thought to reflect an attentional modulation unrelated to the specific task being performed (Broyd, et al. 2009).

Though characterized by higher activity at rest as compared to during task, the DMN was originally identified by its resting state functional connectivity (Greicius, et al. 2003). Functional connectivity, also known as time-series correlations between regions of interest, can be measured at rest (spontaneous) or during task (activation-related) to determine cognitive co-activity. Such correlations between specific regions can be positive, indicating higher network connectivity/integration, or negative (anti-correlation), indicating competitive or complementary function (Fox, et al. 2005; Fransson, et al. 2006). High positive functional connectivity is often observed between homologous regions in the contralateral hemisphere (Stephan, et al. 2007; Clarke, et al. 1994; Rissman, et al. 2004). With regards to the DMN, alterations in resting state functional connectivity, as well as task-related activity, have been noted in several patient populations (Mevel, et al. 2010; Broyd, et al. 2009; Damoiseaux, et al. 2009).

Recently, Sonuga-Barke and Castellanos hypothesized that the attenuation of DMN activity during cognitive demand is a point of dysfunction in those prone to attentional lapse (2007). Their “default mode interference hypothesis” posits that as attention to a cognitive task lessens, DMN deactivation also lessens, such that DMN activity is persistent in the task-active state and thus interferes with task performance. Task-induced DMN deactivation has been studied in several populations with dysfunctions of attention, including schizophrenia, Alzheimer’s disease, normal aging, and autism spectrum disorder (Kennedy, et al. 2006; Persson, et al. 2007; Pomarol-Clotet, et al. 2008; Rombouts, et al. 2005). While PAE is known to result in cognitive task-related attentional problems, such as increased distractibility and longer reaction times (Shaywitz, et al. 1981; Simmons, et al. 2002; Streissguth, et al. 1986), it is unclear whether these outcomes contribute to the general cognitive deficits seen in the population. Examination of task-related deactivation patterns with PAE could reveal whether attentional modulation is contributing to poorer task performance.

Previously, we identified arithmetic processing dysfunction with PAE by reduced task performance and activation in arithmetic processing centers (Santhanam, et al. 2009). In the present study, we examined “deactivation” (i.e., inhibition during higher cognitive demand) of the DMN during the arithmetic task (using a letter-matching task, which requires less cognitive demand, as baseline). Given known attentional problems and the lower task performance and activation reported in the prior study, we expected less deactivation in the DMN in affected groups as compared to control groups. Additionally, given known white matter alterations in several areas of the brain caused by PAE, we examined structural and functional connectivity of the DMN by diffusion tensor imaging (DTI) and resting state fMRI signal correlation, respectively. We expected reduced correlation at rest between DMN regions (namely the MPFC, PCC, and bilateral IPL) in groups with PAE as compared to controls. Furthermore, as the underlying DMN structure has been shown to reflect its functional connectivity (Greicius, et al. 2009; van den Heuvel, et al. 2008), we anticipated a correlative relationship between the DTI and resting state synchrony measures.

2. METHODS

2.1 Participants

Participants were young adults recruited from a longitudinal cohort, derived from a predominantly African-American, low socio-economic status (SES) population, first identified in the prenatal period between 1979 and 1986 (Smith, et al. 1986). All participants were aged 18-24 at the time of participation. Participants were part of a longitudinal study with large-scale follow-ups at birth, 7 years, mid-adolescence, and young adulthood. Participants (and guardians, if necessary) gave informed consent to continue to participate in the research when recontacted as adults. From the longitudinal cohort, three groups were selected for participation in the current study based on prenatal maternal reports of alcohol use in pregnancy and Dysmorphia Checklist (Coles, et al. 1985) ratings. This Checklist, which was developed for use in the initial infancy study, is similar to that used by other investigators (Jones, et al. 2006; Hoyme et al, 2005). It was administered without knowledge of the participants' alcohol exposure status by a pediatric geneticist or a nurse trained by this geneticist and included a weighted list of 30 physical characteristics associated with prenatal alcohol exposure. Those that are considered to be sentinel features of FAS (e.g., absent/ indistinct philtrum; short palpebral fissures) are weighted as "3" while other characteristics that are observed in FASD may be weighted as 2 (e.g.,ptosis, hypoplastic mandible) or 1 (e.g., clinodactyly). Weighted scores are then summed to yield a total score. Validity of this measure has been measured by correlation with alcohol use levels reported by mothers (Coles, et al. 1997) and reliability by test-retest assessments in a clinical setting (Blackston, et al., 2004). This measure has been used consistently throughout this longitudinal study. The ratings were completed at follow-up evaluations at birth, 7 years, and mid-adolescence.

Groups were defined as follows: 1) Exposed, positive for dysmorphia, (DYS: mother reported use of alcohol during pregnancy and the participant received a dysmorphia rating that was at least one standard deviation above the mean at one of the three evaluations); 2) Exposed, without dysmorphia (Non-DYS: mother reported use of alcohol during pregnancy and the participant received no dysmorphia ratings that were one standard deviation above the mean); and 3) Unexposed controls (CON: mother reported no use of alcohol during pregnancy) from the same SES population. Demographical information for these groups is given in Table 1. The mean ounces of absolute alcohol consumption per week of pregnancy for groups 1 and 2 were 13.8 (sd=13.4) and 7.7 (sd=13.3), respectively (Table 1). Before imaging was done, potential participants who were left handed or had some risk during the MRI procedure (e.g., due to pregnancy or metal in the body) were excluded. Additionally, certain subjects were excluded post-imaging from each analysis described below due to excessive head motion or artifact. As a result, the number of subjects in the final analyses were as follows: Resting-state analysis: DYS n=21, Non-DYS n=21, CON n=22; Functional (arithmetic) task analysis: DYS n=19, Non-DYS n=18, CON n=18; and DTI analysis: DYS n=28, Non-DYS n=29, CON n=25. As image analyses spanned multiple modalities, the analytic steps are summarized in the Figure 1 flowchart.

Participants whose data were used in each substudy analysis were compared on the same variables to those whose data was not used in the substudy but were in the full pool (i.e., the union of participants used in any substudy); few significant differences occurred. Participants in the arithmetic analysis and the DTI analysis were likely to report currently drinking less alcohol than those who were not included in each of these analyses. It can be noted that none of the groups showed high alcohol usage (mean alcohol use for the participating groups was in the 1-2 drinks/week range while that for the non-participating groups was in the 3-4 drinks/week range). Participants were significantly younger than non-participants in the arithmetic analysis and the resting state analysis,; the differences between mean ages for participating and non-participating groups was ≤ 1 year in each analysis.

2.2 Experimental Design

All data, including DTI, resting state, and the arithmetic run, were collected in a single imaging session. For the resting state scan, participants were asked only to gaze at a fixation cross. The arithmetic task was block-design, involving alternating between a letter-matching control task (10 consecutive presentations) and a subtraction task (10 consecutive presentations). Five blocks of each task, with questions in random order in each block, were administered over 5 minutes. Visual presentation of the stimulus was similar to Figure 2. Participants saw instructions stating either “Name the letter” or “Subtract from 11” shown before each block, and were then asked to choose (based on the top letter/number) between two letters or numbers on the bottom half of the screen by pressing the left or right button on a response box. The paradigm is described in further detail in our previous publication (Santhanam, et al. 2009).

2.3 Image Acquisition

All images were acquired on a 3T Siemens Trio scanner (Siemens Medical Solutions, Erlangen, Germany). Both the functional and resting state scans used single-shot T2*-weighted echo planar imaging (EPI) sequences with the following parameters: functional run: 34 contiguous axial slices, 3 mm thickness, TR/TE/FA/FOV of 3000ms/32ms/90°/22cm, scan time of 5:06 min, 102 time points; resting state run: 10 contiguous axial slices, 5 mm thickness, TR/TE/FA/FOV 750ms/34ms/50°/22cm, scan time of 3:34 min, 280 time points. DTI data were acquired using a diffusion-weighted EPI sequence with the following parameters: gradients applied in 12 directions (4 averages) with b-value of 1000 s/mm2, 34 contiguous axial slices, 2mm thickness, TR/TE/FOV of 7700ms/90ms/22cm, scan time of 7:08 min.

2.4 Image Analysis: fMRI

FMRI analysis was performed in AFNI (http://afni.nimh.nih.gov/afni). Preprocessing included slice timing correction, volume registration, band pass filtering (resting data only), signal normalization (functional data only), and 5mm FWHM Gaussian blur. Additionally, multiple linear regression of the resting state data was done to remove contributions from head motion (6 parameters: x, y, z displacements and roll, pitch, yaw rotations), white matter, cerebrospinal fluid, and whole brain signals (Fox, et al. 2005). Recently, the regression of whole brain signal from resting-state data has become controversial as it is thought to introduce anti-correlated networks into functional connectivity measures (Murphy, et al. 2009). However, a recent report quantifying the effect of various pre-processing steps on connectivity measures determined that while using global signal regression does introduce anti-correlations, it also approximately doubles the sensitivity to positive correlations and is therefore recommended (Weissenbacher, et al. 2009). Given the ongoing debate, we chose to analyze the data both with and without global regression.

In order to identify regions of deactivation during higher cognition, a general linear model was derived using the letter-matching task as the baseline and arithmetic task blocks as the stimulations. Convolution of the boxcar stimulation functions with a standard impulse response function ($y=t^b \times \exp(-t/c)$, where b and c are constants) produced the main regressor (Cohen 1997). The 6 head motion parameters were used as additional regressors, and the output of the regression analysis (group activation maps) was generated by Talairach transformation (Talairach and Tournoux 1988) of the functional data to common space and averaging across all subjects. To account for multiple comparisons, voxel-wise and cluster thresholding were applied. Monte Carlo simulation revealed that these thresholds corresponded to a false-positive discovery rate (alpha) of less than 1%.

Clusters of significant deactivation (with voxel-wise thresholding of $p<0.05$ and cluster thresholding of 5 contiguous voxels) at the MPFC and PCC were identified. These regions of interest (ROIs) were identified based on the thresholded maps and previously established studies of DMN network nodes. Further, it was verified that the ROIs generally overlapped with the AFNI Talairach atlas, though individual activation maps were used for subsequent analysis due to variability in head size among the PAE population. While negative activity was also seen in other DMN-related regions, these two (MPFC and PCC) were chosen for deactivation quantification purposes because they had the most consistent statistically significant clusters on the individual subject level; additionally, bilateral IPL was specifically not used in quantification due to involvement of this region in task-positive arithmetic processing (Santhanam, et al. 2009). Differences in deactivation between the letter matching and arithmetic tasks were determined by extracting and averaging the regression coefficients from the clusters identified as the MPFC and PCC, respectively. Deactivation differences in each ROI were examined independently given recent findings of unique functional specialization for each of these two DMN loci (Uddin, et al. 2009). These clusters were chosen as their robust activity and connectivity within the DMN is well-established (Greicius, et al. 2003; Margulies, et al. 2007). Group maps were generated to visualize the deactivation in each group over the MPFC and PCC regions, respectively (voxel-wise thresholding of $p<0.05$ and cluster thresholding of 4 contiguous voxels). Due to considerable head size differences in the PAE population, the deactivation clusters from the group activation map were masked and back-projected into native space for each subject for quantification of the deactivation difference. Average unthresholded regression coefficients were converted to percent signal change and compared between groups by t-test. To further verify a relationship between DMN deactivation seen during the arithmetic task and attentional modulation, the percent signal change (absolute value) over the MPFC and PCC regions combined was correlated with performance (i.e., accuracy) on the arithmetic task.

Using the deactivation cluster as a mask, corresponding PCC regions in the resting state were extracted for each individual in native space, and correlation maps were derived. Voxel-wise thresholding of $p<0.001$ and cluster threshold of 4 contiguous voxels (corresponding to multiple comparisons correction of alpha<1% by Monte Carlo simulation) were used. An average map of correlation for all subjects revealed significant correlation clusters in the MPFC and bilateral IPL regions, using PCC as the seed. Correlation maps for each group were also rendered to visually examine group differences (voxel-wise threshold of $p<0.01$ and cluster threshold of 4 contiguous voxels). Masks of MPFC and IPL regions from this group-level map were back-projected to native space for each individual, and the average correlation coefficient was extracted over the masked region and compared between groups by t-test. Additionally, to examine whether differences exist in signal amplitude in DMN regions (i.e., those that survived the correlation map threshold), mean signal intensity over the resting state run was compared between groups (Xu, et al. 2006; Yang, et al. 2007).

2.5 Image Analysis: DTI

Voxel-wise analysis of DTI data was performed using the tract-based spatial statistics (TBSS) program from FSL 4.0 (http://www.fmrib.ox.ac.uk/fsl/). TBSS offers the advantage of non-linear registration followed by projection onto an alignment-invariant white matter "skeleton." It was chosen because TBSS is less reliant on image registration between subjects for comparison (Smith, et al. 2006) and was previously shown to elucidate differences between exposed and control groups from the same cohort in subregions of the corpus callosum (Li, et al. 2009). Briefly, a FA template specific to the PAE population in this study was created from the FA images of all subjects. The average FA image was then eroded to form a mean FA skeleton to which the FA map of each individual is aligned. Details of the template creation, skeleton derivation, and alignment can be found in our

previously published study (Li, et al. 2009). Skeletons were derived in the same manner from fractional anisotropy (FA), mean diffusivity (MD), axial diffusivity (AD), and radial diffusivity (RD) maps.

A permutation algorithm (Smith, et al. 2006) that does not require a Gaussian distribution was used to run statistics on the group differences in DTI measures. Parameters were 5000 random permutations and comparisons were corrected to a family-wise (type I) error rate of less than 5%. TFCE (FSL version 4.1) was used in place of voxel-wise or cluster thresholding. TFCE is a relatively new technique that allows for statistical analysis without an initial cluster-forming threshold. In this method, each voxel is given a value corresponding to the sum of the "scores" of its surrounding voxels; the score is determined by the height (increased incrementally from zero to the signal intensity of the given voxel) and extent of the cluster that contains the voxel. TFCE has been shown to improve sensitivity of signal detection, with an optimized height (H=2) and extent (E=0.5). Details of TFCE implementation and validation are provided by Smith and Nichols (2009). As the MPFC and PCC regions are known to be structurally connected via the bilateral cingulum bundles (Greicius, et al. 2009; van den Heuvel, et al. 2008), these major white matter structures were chosen for subsequent ROI analysis of DTI measures. Skeleton-based ROI analysis of the bilateral cingulum bundles was performed by defining the ROI as the intersection of the anatomical bilateral cingulum (as identified by a white matter atlas provided by FSL) and the FA skeleton. The ROI mask was used to extract average FA, MD, AD, and RD over this region. Statistical comparison of these DTI measures in exposed versus controls (t-test) was performed in SPSS 15.0 (SPSS Inc., Chicago, IL).

In order to examine the relationship between structural and functional connectivity of the DMN, correlation between DTI measures over the cingulum and functional synchrony (defined by average correlation coefficient over MPFC region in correlation map with PCC seed) was determined. Statistical analysis was again performed in SPSS 15.0. Pearson's correlation coefficient was reported for each exposure group respectively (n=19 for the control group; n=16 for each the dysmorphic and non-dysmorphic PAE group).

3. RESULTS

Figure 3 is a group average activation map indicating regions of DMN deactivation during the arithmetic task (using the letter-matching task as baseline). The most robust clusters of deactivation were found in the MPFC and PCC regions, identified in the figure. As group-level maps in Figure 4 indicate, deactivation was lower in the dysmorphic PAE group as compared to controls, while the non-dysmorphic group had lower but not-significant deactivation compared to controls. These differences were quantified by percent signal change in the MPFC and PCC, respectively (Table 2). Deactivation was then correlated with task accuracy, which is represented here (as group averages): 72.6%, 65.3% (p=0.104 vs controls), and 60.1% (p=.022 vs controls) for control, non-dysmorphic PAE, and dysmorphic PAE groups, respectively (Santhanam, et al. 2009). The percent signal change over the MPFC and PCC regions combined was found to correlate with accuracy on the arithmetic task for all groups (r=0.361, p=0.037).

The PCC cluster from Figure 3 was then used as a seeding region in the resting-state data to examine functional connectivity. Figure 5 shows the group correlation map using the PCC seed. Significant regions of correlation with the PCC were MPFC and bilateral IPL. Figure 5 indicates similar correlation extent and intensity (without introducing significant anti-correlation in the regions of interest), regardless of global signal regression. . However, global signal regressed data was chosen for subsequent analysis in light of recent evidence that this method increases sensitivity to signal (Weissenbacher, et al. 2009). As a measure of

baseline DMN connectivity, resting functional connectivity between MPFC-PCC and bilateral IPL-PCC regions were examined, respectively. Average correlation coefficients (derived from the Figure 6 statistical map) over the MPFC and bilateral IPL was compared between the control group and each exposure group. The control group appeared to have greater correlation in these regions (positive voxels in Figure 6), and the average correlation coefficients, extracted from the MPFC and IPL regions, are shown in Table 2. Correlation (reflecting resting state DMN synchrony) was significantly greater in the control group as compared to both exposure groups, and the two PAE groups had comparable correlation. Signal amplitude over the resting state time-course was found to be comparable between PAE groups and controls (results not shown; p=0.34 for non-dysmorphic PAE group, p=0.24 for dysmorphic PAE group).

Figure 7 indicates the location of the bilateral cingulum bundles in relation to the deactivation clusters from Figure 3. Figure 8 contains the results of whole-brain TBSS. Differences in FA were detectable at the bilateral cingulum bundle between groups using a family-wise error of less than 5% (pFWE<0.05) and the threshold-free cluster enhancement (TFCE) method for cluster identification. In the subsequent regional skeleton-based ROI analysis (using bilateral cingulum bundles as the ROI), differences between groups in MD and RD were additionally detectable (Table 3). ROI extraction was done to compare differences in average FA, AD, MD, and RD between groups. Both PAE groups had lower FA and higher RD values as compared to controls and additionally the dysmorphic PAE group had a higher MD than controls.

To examine whether structural and functional connectivity were affected in a corresponding manner, correlation between the MPFC-PCC correlation coefficient and DTI measures over the cingulum was determined. A significant positive correlation with FA value was found only for the control group (r=0.571, p=0.033). No significant correlations were found for any other DTI measures.

4. DISCUSSION

Task-related deactivation and structural and functional connectivity of the DMN all appear to be affected by PAE. Dysmorphic PAE individuals had significantly less deactivation in the MPFC and PCC during the arithmetic task as compared to controls. Functional connectivity among the PCC, MPFC, and IPL regions was also lower for both PAE groups as compared to controls at rest, as well as structural connectivity between the PCC and MPFC via the cingulum bundles.

As previously mentioned, deactivation of the DMN has been observed to be altered in several clinical populations. In general, these studies agree that there exists a competition between an extrinsic (cognitive functioning) network and an intrinsic (default mode) network (Clare Kelly, et al. 2008), and that this competition can be a point of dysfunction. For this study, a positive correlation was found between arithmetic task deactivation (i.e., absolute value of percent signal change) and task accuracy, implying a relationship between DMN deactivation and attention to task. Attentional modulation during the arithmetic task appears to be affected for the dysmorphic PAE group in this study, which can be related to their poorer task performance and lower activation in arithmetic centers (previously reported). It should be noted that even without the lowest scoring dysmorphic PAE participants, the reduced activation was still observed (previously reported), implying that the arithmetic centers are at least partially responsible for the lower performance. However, one limitation of this study is that poorer arithmetic performance in the dysmorphic group cannot be attributed in a definite manner to either math skill impairment or task engagement.

Though both deficits can be reported for the dysmorphic PAE group, it is unclear how they contribute to the overall behavioral effect.

The DMN "interference hypothesis" has been further supported by recent studies reporting intrinsic anti-correlation between the DMN and task-related networks in the resting state (Fox, et al. 2005; Fox, et al. 2006; Fransson, et al. 2006). Though the majority of literature on DMN functioning regards the network as homogenous, recently Uddin, et al. has investigated the possibility of unique functional specialization within the DMN (2009). They examined the positively and anti-correlated regions for the ventral medial PFC (vmPFC) and PCC regions, respectively, as these are the most robust nodes of the network. Findings included significant differences in networks anti-correlated with each node, with vmPFC activity anti-correlated with parietal visual spatial and temporal attention networks as compared to PCC activity, which was anti-correlated with motor control networks (Uddin, et al. 2009). Granger causality results also suggested modulation of these loci upon the task-positive activity in these networks. Therefore, the authors speculate that activity in these two DMN loci may independently and uniquely influence task-positive activation in the networks with which they are anti-correlated. As the present study found significant DMN deactivation differences in the MPFC only (and not in the PCC region), it follows that arithmetic task activation would be affected, given the strong reliance on bilateral parietal visual spatial networks for arithmetic processing (Dehaene, et al. 2004; Santhanam, et al. 2009).

Both PAE groups had reduced structural and resting state functional connectivity between the MPFC and PCC. The cingulum bundles connecting these two nodes of the DMN had lower FA and higher RD in both groups, and additionally increased MD in the dysmorphic PAE group. . FA and MD are known measures of white matter integrity (Alexander, et al. 2007; Stebbins, et al. 2009); thus, the lower FA in both groups and higher MD in the dysmorphic group likely reflect significant damage to the cingulum bundles. That both PAE groups also had differences in RD may be indicative of myelin-related insult, as higher RD is associated with demyelination specifically (Klawiter, et al. 2011; Avram, et al. 2010; Song, et al. 2005). Furthermore, the resting state connectivity was reduced in both PAE groups, with comparable signal magnitude among groups confirming a dysfunction of synchrony specifically (Xu, et al. 2006; Yang, et al. 2007).

The non-dysmorphic PAE group had intermediate (but not significant from controls) deactivation of the DMN during the arithmetic task, which accompanies their previously reported intermediate task performance and activation. However, structural and baseline functional connectivity was significantly impaired in this group as compared to controls, with measures more comparable to the dysmorphic PAE group. Additionally, while the functional connectivity of the control group had a positive correlation with FA, the PAE groups did not. Correlation between these measures in the control group implies a relationship between structural and functional connectivity in parts of the DMN in healthy individuals.

This study is the first to examine DMN activity in individuals with prenatal exposure to alcohol. Dysmorphic PAE individuals appear unable to sufficiently deactivate the DMN during cognitive tasks, which could contribute to lesser task-related positive activation, lower task-related attentional modulation, and poorer task performance. Additionally, there appears to be a "disconnect" between nodes of the DMN in individuals with PAE, reflected in reduced structural and functional network connectivity. To our knowledge, this is the first paper to relate structural connectivity, functional connectivity, and task-related deactivation of the DMN in a clinical population. PAE appears to affect all these aspects of the network, implying a global effect on this resting state network and warranting further study.

Examination of other resting state networks would aid in better understanding whether PAE is having a global effect on rest or specifically on the default network. Additionally, it would be interesting to note whether DMN deactivation is dependent on the task type and/or task performance. In the current study, we used an arithmetic task, which is highly cognitively demanding for individuals with PAE, and in our case task performance was lower in affected groups. However it is possible the deactivation patterns would differ with a less demanding task or when task performance is controlled. Finally, this study implies attentional modulation plays a role in cognitive deficit seen with PAE, but more studies controlling for specific types of attentional control and cognition are needed to elucidate the contribution of each to behavioral outcomes.

Acknowledgments

This work was supported by Georgia Research Alliance and by the National Institute of Alcohol and Alcoholism (NIAAA) RO1 AA014373. We thank Sharron Paige-Whitaker for her work corresponding with and recruiting participants. We would also like to thank the study participants and their families for their continuing cooperation with this research.

REFERENCES

Alexander AL, Lee JE, et al. Diffusion tensor imaging of the brain. Neurotherapeutics. 2007; 4(3): 316–329. [PubMed: 17599699]

Avram AV, Guidon A, et al. Myelin water weighted diffusion tensor imaging. Neuroimage. 2010; 53(1):132–138. [PubMed: 20587369]

Blackston, RD.; Coles, CD.; Kable, JA.; Seitz, R. Reliability and validity of the Dysmorphia Checklist: Relating severity of dysmorphia to cognitive and behavioral outcomes in children with prenatal alcohol exposure. Poster presented at the American Society of Human Genetics Annual Meeting; Toronto, Canada. 2004.

Broyd SJ, Demanuele C, Debener S, Helps SK, James CJ, Sonuga-Barke EJ. Default-mode brain dysfunction in mental disorders: a systematic review. Neurosci Biobehav Rev. 2009; 33(3):279–96. [PubMed: 18824195]

Clare Kelly AM, Uddin LQ, Biswal BB, Castellanos FX, Milham MP. Competition between functional brain networks mediates behavioral variability. Neuroimage. 2008; 39(1):527–37. [PubMed: 17919929]

Clarke JM, Zaidel E. Anatomical-behavioral relationships: corpus callosum morphometry and hemispheric specialization. Behav Brain Res. 1994; 64(1-2):185–202. [PubMed: 7840886]

Cohen MS. Parametric analysis of fMRI data using linear systems methods. Neuroimage. 1997; 6(2): 93–103. [PubMed: 9299383]

Coles CD, Platzman KA, Raskind-Hood CL, Brown RT, Falek A, Smith IE. A comparison of children affected by prenatal alcohol exposure and attention deficit, hyperactivity disorder. Alcohol Clin Exp Res. 1997; 21(1):150–61. [PubMed: 9046388]

Coles CD, Smith I, Fernhoff PM, Falek A. Neonatal neurobehavioral characteristics as correlates of maternal alcohol use during gestation. Alcohol Clin Exp Res. 1985; 9(5):454–60. [PubMed: 3904511]

Conry J. Neuropsychological deficits in fetal alcohol syndrome and fetal alcohol effects. Alcohol Clin Exp Res. 1990; 14(5):650–5. [PubMed: 2264592]

Damoiseaux JS, Greicius MD. Greater than the sum of its parts: a review of studies combining structural connectivity and resting-state functional connectivity. Brain Struct Funct. Oct; 2009 213(6):525–33. 2009. [PubMed: 19565262]

Dehaene S, Molko N, Cohen L, Wilson AJ. Arithmetic and the brain. Curr Opin Neurobiol. 2004; 14(2):218–24. [PubMed: 15082328]

Fox MD, Corbetta M, et al. Spontaneous neuronal activity distinguishes human dorsal and ventral attention systems. Proc Natl Acad Sci U S A. 2006; 103(26):10046–10051. [PubMed: 16788060]

Fox MD, Snyder AZ, Vincent JL, Corbetta M, Van Essen DC, Raichle ME. The human brain is intrinsically organized into dynamic, anticorrelated functional networks. Proc Natl Acad Sci U S A. 2005; 102(27):9673–8. [PubMed: 15976020]

Fransson P. How default is the default mode of brain function? Further evidence from intrinsic BOLD signal fluctuations. Neuropsychologia. 2006; 44(14):2836–2845. [PubMed: 16879844]

Fransson P. Spontaneous low-frequency BOLD signal fluctuations: an fMRI investigation of the resting-state default mode of brain function hypothesis. Hum Brain Mapp. Sep; 2005 26(1):15–29. [PubMed: 15852468]

Fryer SL, Tapert SF, Mattson SN, Paulus MP, Spadoni AD, Riley EP. Prenatal alcohol exposure affects frontal-striatal BOLD response during inhibitory control. Alcohol Clin Exp Res. Aug; 2007 31(8):1415–24. [PubMed: 17559542]

Golland Y, Golland P, Bentin S, Malach R. Data-driven clustering reveals a fundamental subdivision of the human cortex into two global systems. Neuropsychologia. 2008; 46(2):540–53. [PubMed: 18037453]

Greicius MD, Krasnow B, Reiss AL, Menon V. Functional connectivity in the resting brain: a network analysis of the default mode hypothesis. Proc Natl Acad Sci U S A. 2003; 100(1):253–8. [PubMed: 12506194]

Greicius MD, Supekar K, Menon V, Dougherty RF. Resting-state functional connectivity reflects structural connectivity in the default mode network. Cereb Cortex. 2009; 19(1):72–8. [PubMed: 18403396]

Guerri C, Bazinet A, Riley EP. Foetal Alcohol Spectrum Disorders and alterations in brain and behaviour. Alcohol Alcohol. 2009; 44(2):108–14. [PubMed: 19147799]

Hoyme HE, May PA, et al. A practical clinical approach to diagnosis of fetal alcohol spectrum disorders: clarification of the 1996 institute of medicine criteria. Pediatrics. 2005; 115(1):39–47. [PubMed: 15629980]

Jones KL, Robinson LK, et al. Accuracy of the diagnosis of physical features of fetal alcohol syndrome by pediatricians after specialized training. Pediatrics. 2006; 118(6):e1734–1738. [PubMed: 17088402]

Kennedy DP, Redcay E, Courchesne E. Failing to deactivate: resting functional abnormalities in autism. Proc Natl Acad Sci U S A. 2006; 103(21):8275–80. [PubMed: 16702548]

Klawiter EC, Schmidt RE, et al. Radial diffusivity predicts demyelination in ex vivo multiple sclerosis spinal cords. Neuroimage. 2011

Li L, Coles CD, Lynch ME, Hu X. Voxelwise and skeleton-based region of interest analysis of fetal alcohol syndrome and fetal alcohol spectrum disorders in young adults. Hum Brain Mapp. 2009; 30(10):3265–74. [PubMed: 19278010]

Malisza KL, Allman AA, Shiloff D, Jakobson L, Longstaffe S, Chudley AE. Evaluation of spatial working memory function in children and adults with fetal alcohol spectrum disorders: a functional magnetic resonance imaging study. Pediatr Res. 2005; 58(6):1150–7. [PubMed: 16306185]

Margulies DS, Kelly AM, Uddin LQ, Biswal BB, Castellanos FX, Milham MP. Mapping the functional connectivity of anterior cingulate cortex. Neuroimage. 2007; 37(2):579–88. [PubMed: 17604651]

Mattson SN, Riley EP. A review of the neurobehavioral deficits in children with fetal alcohol syndrome or prenatal exposure to alcohol. Alcohol Clin Exp Res. 1998; 22(2):279–94. [PubMed: 9581631]

Mattson SN, Riley EP, Gramling L, Delis DC, Jones KL. Neuropsychological comparison of alcohol-exposed children with or without physical features of fetal alcohol syndrome. Neuropsychology. 1998; 12(1):146–53. [PubMed: 9460742]

McKiernan KA, D'Angelo BR, Kaufman JN, Binder JR. Interrupting the "stream of consciousness": an fMRI investigation. Neuroimage. 2006; 29(4):1185–91. [PubMed: 16269249]

Meintjes EM, Jacobson JL, Molteno CD, Gatenby JC, Warton C, Cannistraci CJ, Hoyme HE, Robinson LK, Khaole N, Gore JC, Jacobson SW. An FMRI study of number processing in children with fetal alcohol syndrome. Alcohol Clin Exp Res. Aug; 2010 34(8):1450–64. [PubMed: 20528824]

Mevel K, Grassiot B, et al. The default mode network: cognitive role and pathological disturbances. Rev Neurol (Paris). 2010; 166(11):859–872. [PubMed: 20226489]

Murphy K, Birn RM, Handwerker DA, Jones TB, Bandettini PA. The impact of global signal regression on resting state correlations: are anti-correlated networks introduced? Neuroimage. 2009; 44(3):893–905. [PubMed: 18976716]

Olson HC, Feldman JJ, Streissguth AP, Sampson PD, Bookstein FL. Neuropsychological deficits in adolescents with fetal alcohol syndrome: clinical findings. Alcohol Clin Exp Res. 1998; 22(9): 1998–2012. [PubMed: 9884144]

Persson J, Lustig C, Nelson JK, Reuter-Lorenz PA. Age differences in deactivation: a link to cognitive control? J Cogn Neurosci. 2007; 19(6):1021–32. [PubMed: 17536972]

Pomarol-Clotet E, Salvador R, Sarro S, Gomar J, Vila F, Martinez A, Guerrero A, Ortiz-Gil J, Sans-Sansa B, Capdevila A. Failure to deactivate in the prefrontal cortex in schizophrenia: dysfunction of the default mode network? Psychol Med. 2008; 38(8):1185–93. others. [PubMed: 18507885]

Rombouts SA, Barkhof F, Goekoop R, Stam CJ, Scheltens P. Altered resting state networks in mild cognitive impairment and mild Alzheimer's disease: an fMRI study. Hum Brain Mapp. 2005; 26(4):231–9. [PubMed: 15954139]

Santhanam P, Li Z, Hu X, Lynch ME, Coles CD. Effects of Prenatal Alcohol Exposure on Brain Activation During an Arithmetic Task: An fMRI Study. Alcohol Clin Exp Res. 2009

Shaywitz SE, Caparulo BK, Hodgson ES. Developmental language disability as a consequence of prenatal exposure to ethanol. Pediatrics. 1981; 68(6):850–5. [PubMed: 7322723]

Simmons RW, Wass T, Thomas JD, Riley EP. Fractionated simple and choice reaction time in children with prenatal exposure to alcohol. Alcohol Clin Exp Res. 2002; 26(9):1412–9. [PubMed: 12351937]

Singh KD, Fawcett IP. Transient and linearly graded deactivation of the human default-mode network by a visual detection task. Neuroimage. 2008; 41(1):100–12. [PubMed: 18375149]

Smith IE, Coles CD, Lancaster J, Fernhoff PM, Falek A. The effect of volume and duration of prenatal ethanol exposure on neonatal physical and behavioral development. Neurobehav Toxicol Teratol. 1986; 8(4):375–81. [PubMed: 3762847]

Smith SM, Jenkinson M, Johansen-Berg H, Rueckert D, Nichols TE, Mackay CE, Watkins KE, Ciccarelli O, Cader MZ, Matthews PM. Tract-based spatial statistics: voxelwise analysis of multi-subject diffusion data. Neuroimage. 2006; 31(4):1487–505. others. [PubMed: 16624579]

Smith SM, Nichols TE. Threshold-free cluster enhancement: addressing problems of smoothing, threshold dependence and localisation in cluster inference. Neuroimage. 2009; 44(1):83–98. [PubMed: 18501637]

Song SK, Yoshino J, et al. Demyelination increases radial diffusivity in corpus callosum of mouse brain. Neuroimage. 2005; 26(1):132–140. [PubMed: 15862213]

Sonuga-Barke EJ, Castellanos FX. Spontaneous attentional fluctuations in impaired states and pathological conditions: a neurobiological hypothesis. Neurosci Biobehav Rev. 2007; 31(7):977–86. [PubMed: 17445893]

Sowell ER, Lu LH, O'Hare ED, McCourt ST, Mattson SN, O'Connor MJ, Bookheimer SY. Functional magnetic resonance imaging of verbal learning in children with heavy prenatal alcohol exposure. Neuroreport. 2007; 18(7):635–9. [PubMed: 17426589]

Spadoni AD, Bazinet AD, Fryer SL, Tapert SF, Mattson SN, Riley EP. BOLD response during spatial working memory in youth with heavy prenatal alcohol exposure. Alcohol Clin Exp Res. Dec; 2009 33(12):2067–76. [PubMed: 19740135]

Stebbins GT, Murphy CM. Diffusion tensor imaging in Alzheimer's disease and mild cognitive impairment. Behav Neurol. 2009; 21(1):39–49. [PubMed: 19847044]

Stephan KE, Fink GR, et al. Mechanisms of hemispheric specialization: insights from analyses of connectivity. Neuropsychologia. 2007; 45(2):209–228. [PubMed: 16949111]

Streissguth AP, Barr HM, Sampson PD, Parrish-Johnson JC, Kirchner GL, Martin DC. Attention, distraction and reaction time at age 7 years and prenatal alcohol exposure. Neurobehav Toxicol Teratol. 1986; 8(6):717–25. [PubMed: 3808187]

Talairach, J.; Tournoux, P. Co-planar stereotaxic atlas of the human brain. Thieme Medical Publishers, Inc.; New York: 1988.

Uddin LQ, Kelly AM, Biswal BB, Castellanos F Xavier, Milham MP. Functional connectivity of default mode network components: correlation, anticorrelation, and causality. Hum Brain Mapp. 2009; 30(2):625–37. [PubMed: 18219617]

van den Heuvel M, Mandl R, Luigjes J, Pol H Hulshoff. Microstructural organization of the cingulum tract and the level of default mode functional connectivity. J Neurosci. 2008; 28(43):10844–51. [PubMed: 18945892]

Weissenbacher A, Kasess C, Gerstl F, Lanzenberger R, Moser E, Windischberger C. Correlations and anticorrelations in resting-state functional connectivity MRI: a quantitative comparison of preprocessing strategies. Neuroimage. 2009; 47(4):1408–16. [PubMed: 19442749]

Weissman DH, Roberts KC, Visscher KM, Woldorff MG. The neural bases of momentary lapses in attention. Nat Neurosci. 2006; 9(7):971–8. [PubMed: 16767087]

Wilson SM, Molnar-Szakacs I, Iacoboni M. Beyond superior temporal cortex: intersubject correlations in narrative speech comprehension. Cereb Cortex. 2008; 18(1):230–42. [PubMed: 17504783]

Xu G, Xu Y, Wu G, Antuono PG, Hammeke TA, Li SJ. Task-modulation of functional synchrony between spontaneous low-frequency oscillations in the human brain detected by fMRI. Magn Reson Med. 2006; 56(1):41–50. [PubMed: 16767759]

Yang H, Long XY, Yang Y, Yan H, Zhu CZ, Zhou XP, Zang YF, Gong QY. Amplitude of low frequency fluctuation within visual areas revealed by resting-state functional MRI. Neuroimage. 2007; 36(1):144–52. [PubMed: 17434757]

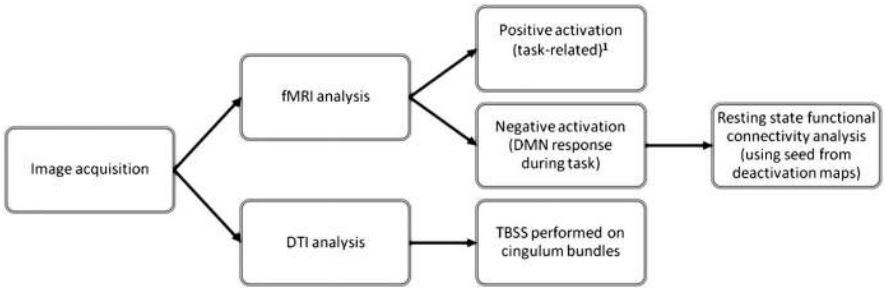

Figure 1. Flowchart of the steps of image analysis in the present study

1: indicates analysis performed in previously published study (Santhanam, et al. 2009).

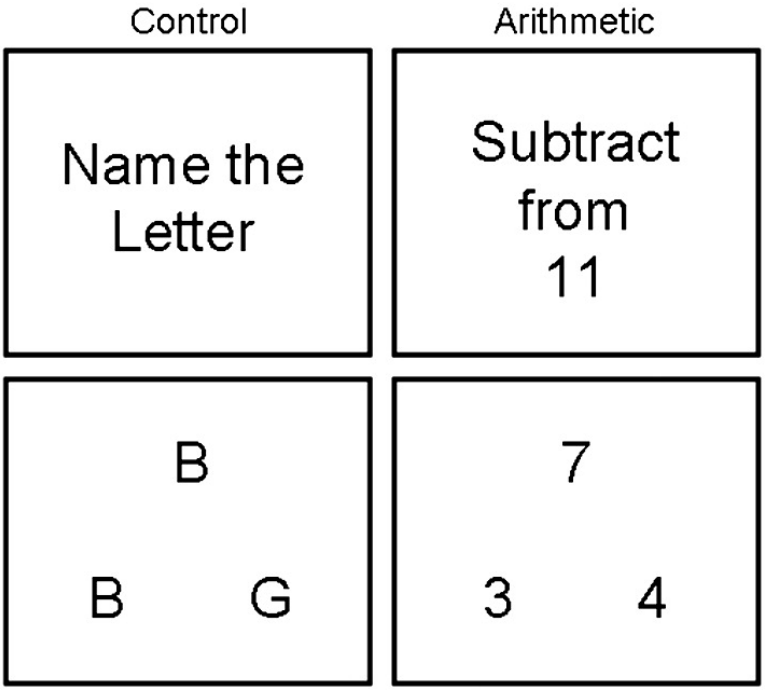

Figure 2.
Example of visual presentation of arithmetic task.

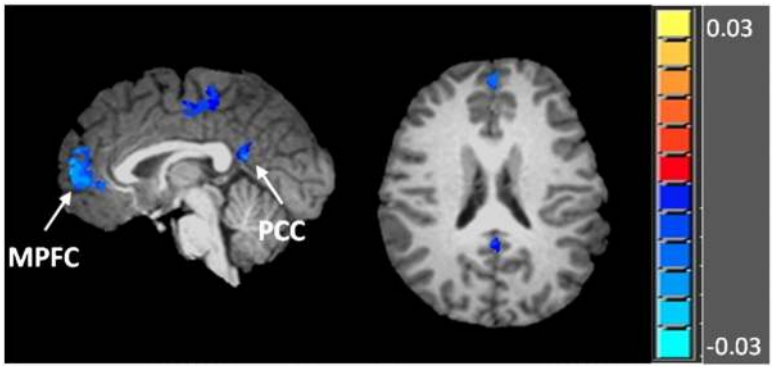

Figure 3. Regions of default mode deactivation during arithmetic task using letter-matching task as baseline

MPFC and PCC clusters from these average activation maps (of all subjects included in functional task analysis; $p<0.05$ and cluster threshold of 5 contiguous voxels) were used for subsequent resting-state analysis. Color bar (also applicable to Figure 4) indicates these regions are negatively activated.

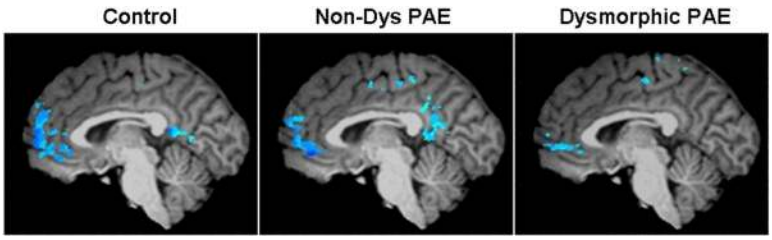

Figure 4. Group maps of default mode deactivation

Regions of significant deactivation in control, non-dysmorphic PAE, and dysmorphic PAE groups. Voxel-wise threshold was $p<0.05$ with a cluster threshold of 4 contiguous voxels.

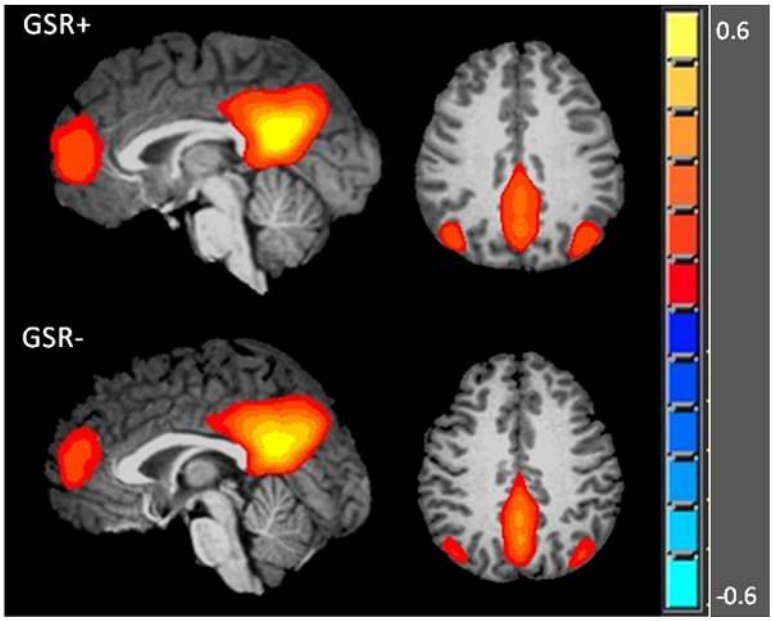

Figure 5. Resting-state functional connectivity group maps

Resting correlation maps with (GSR+) and without (GSR−) global signal regression. At threshold $p<0.001$, only positive correlation (red-yellow: see color bar in Figure 1) was noted with the seeding region regardless of regression method. Seeding was in the PCC region defined in Figure 1. Color bar (also applicable to Figure 6) indicates these regions have robust positive correlation.

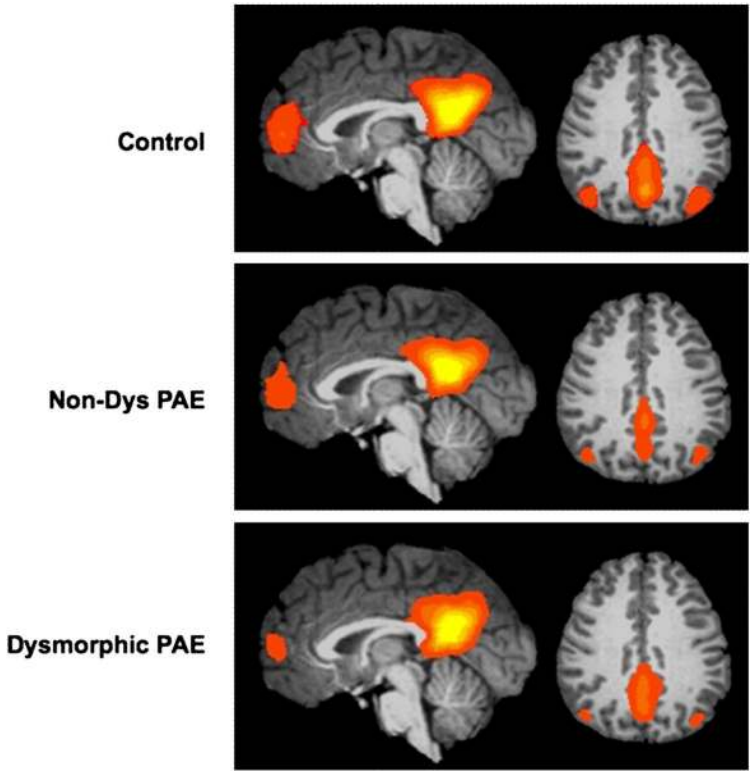

Figure 6. Group maps of resting-state correlation

Seeding-correlation maps for control, non-dysmorphic PAE, and Dysmorphic PAE groups. Seed was the PCC region identified in Figure 1. Notable regions of significant correlation are MPFC and bilateral IPL for all groups. Threshold used was $p<0.01$ and 4 contiguous voxels.

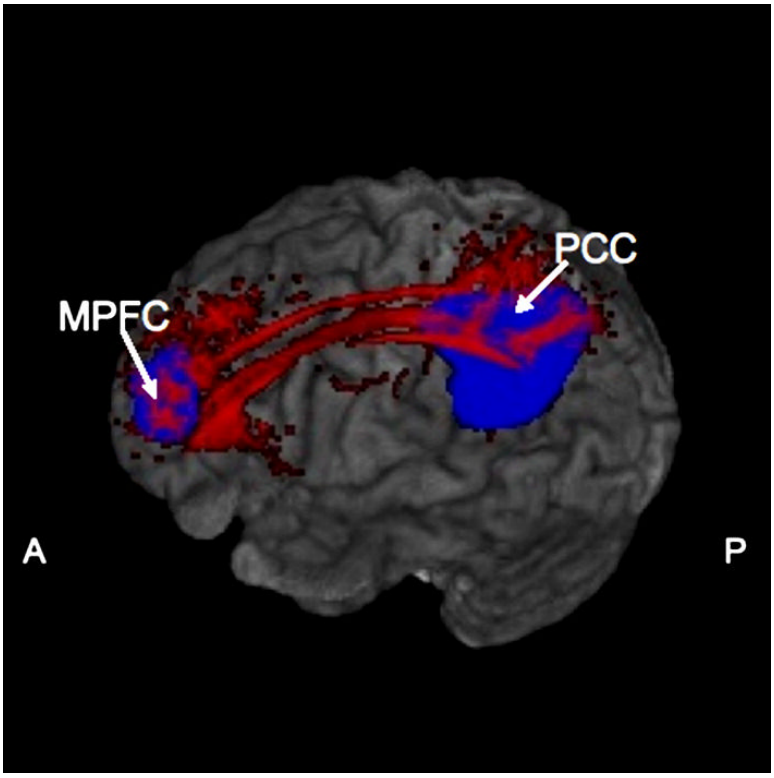

Figure 7. Structural connectivity of default mode network nodes

Three-dimensional rendering of MPFC and PCC regions of deactivation (blue) and bilateral cingulum bundles connecting them (red). Figure reflects deactivation regions from Figure 1 and bilateral cingulum bundles from mean FA skeleton (for all subjects included in DTI analysis). A,P = indicate anterior and posterior directions in image.

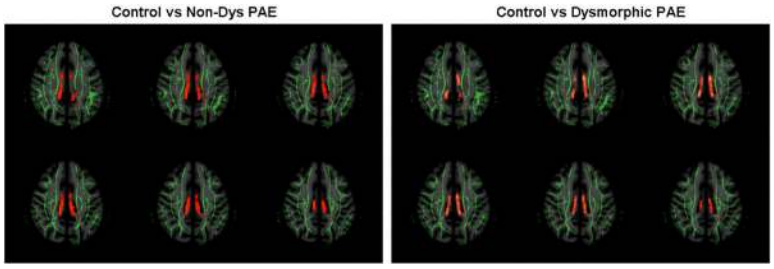

Figure 8. TBSS results indicating FA differences in bilateral cingulum

Regions of significant difference in FA between control and non-dysmorphic PAE groups and control and dysmorphic PAE groups are shown. Green indicates mean FA skeleton and red indicates regions of significant difference between groups, with thickened red-yellow for the bilateral cingulum ROI. Axial slices shown are z=107 to z=112.

Table 1

Demographic and prenatal exposure variables for participants (n=96) by exposure group.

Variable	Group			Statistic	Significance
	Control (n= 28)[a]	NonDys(n= 34)[a]	Dys (n= 34)[a]		
Gender – % male	46.4	20.6	50.0	$x^2_{(2)}$=7.246	p=.027
Ethnicity – % African-American	100	97.1	100	$x^2_{(2)}$=1.843	n.s.
Age at imaging, M (SD)	22.8 (1.7)	22.9 (1.7)	23.0 (2.1)	$F_{(2,93)}$=.222	n.s.
Monthly income – $ in past 30 days, M (SD) *n*=94	1217 (1704)	624 (419)	1105 (1026)	$F_{(2,91)}$=2.502	p=.088
Education completed – years, M (SD) *n*=95	12.1 (1.6)	11.6 (1.5)	11.9 (1.6)	$F_{(2,92)}$=.753	n.s.
Full-scale IQ [b], M (SD) *n*=95	84.2 (8.7)	79.8 (11.4)	77.3 (11.6)	$F_{(2,92)}$=3.094	p=.050 Dys < Control[c]
Dysmorphia rating at adult visit, M (SD) *n*=95	3.5 (3.3)	4.2 (3.6)	9.5 (7.3)	$F_{(2,92)}$=12.911	p=.000; Dys > Control, NonDys[c]
Current alcohol use by participant (oz/AA/wk)[d], M (SD) *n*=95	1.2 (2.7)	1.2 (1.7)	1.1 (1.8)	$F_{(2,92)}$=.017	n.s.
Amount of alcohol exposure during pregnancy (oz/AA/wk)[d], M (SD)	0 (0)	7.7 (13.4)	14.0 (13.2)	$F_{(2,93)}$=11.979	p=.000; Control < Dys, NonDys[c]
Cigarettes during pregnancy – % using	32.1	61.8	85.3	$x^2_{(2)}$=18.315	p=.000
Marijuana during pregnancy – % using	17.9	35.3	26.5	$x^2_{(2)}$=2.374	n.s.
Cocaine during pregnancy – % using *n*=92	0	17.6	6.7	$x^2_{(2)}$=6.254	p=.044

[a] = if data for a variable are not available for some participants, the *n* used for the analysis is noted next to the variable name

[b] = WASI IQ obtained at current testing

[c] = post hoc comparisons completed with Tukey HSD test.

Table 2

Comparison of resting-state DMN correlation and task-based DMN deactivation between control and PAE groups.

Connectivity/Activation Measure	Control	Non-Dys PAE	Dysmorphic PAE
Percent Signal Change in MPFC (SEM)	−0.808 (0.087)	−0.789 (0.094)	−0.604* (0.098)
Percent Signal Change in PCC (SEM)	−0.265 (0.095)	−0.168 (0.060)	−0.174 (0.110)
Mean Correlation Coefficient in MPFC and IPL using PCC seed: with GSR (SEM)	0.256 (0.060)	0.185* (0.036)	0.194* (0.042)
Mean Correlation Coefficient in MPFC and IPL using PCC seed: without GSR (SEM)	0.405 (0.036)	0.316* (0.019)	0.321* (0.024)

* = significantly different from control group by t-test ($p<0.05$)

SEM = standard error of the mean

GSR = global signal regression.

Table 3

Comparison of DTI measures between control and PAE groups by skeleton-based ROI analysis of bilateral cingulum.

Mean over cingulum bundles	Control	Non-Dys PAE	Dysmorphic PAE
FA (SEM)	0.570 (0.008)	0.539* (0.007)	0.545* (0.008)
MD (SEM)	0.731 (0.006)	0.742 (0.009)	0.750* (0.008)
AD (SEM)	1.265 (0.012)	1.241 (0.015)	1.273 (0.012)
RD (SEM)	0.464 (0.008)	0.492* (0.009)	0.491* (0.011)

FA = fractional anisotropy

MD = mean diffusivity ($x10^{-3}$ mm^2/s)

AD = axial diffusivity $\lambda 1$ ($x10^{-3}$ mm^2/s)

RD = radial diffusivity $\lambda 2+\lambda 3/2$ ($x10^{-3}$ mm^2/s)

* = significantly different from control group by t-test ($p<0.05$)

SEM = standard error of the mean.